Retrospective Study

Infrared Thermography: Clinical Value for Diagnosing Persistent Somatoform Pain Disorders?

Zhuoshan Zou, BS, Shuang Zeng, BS, JunTong Tang, BS, Zhenzhen Fan, MD, and Jian Cui, MD, PhD

From: Army Medical University, Chongqing, China

Address Correspondence:
Jian Cui, MD, PhD
Army Medical University
Department of Pain Medicine,
First Affiliated Hospital
No 30 Gaotanyan Street,
Shapingba District
Chongqing, 400038, China
E-mail: cqjian211@163.com

Disclaimer: This study was funded by National Natural Science Foundation of China (No 81870883) and 2019 Chongqing Clinical Key Specialty Construction Project Funding (CQZDZK001).

Conflict of interest: Each author certifies that he or she, or a member of his or her immediate family, has no commercial association (i.e., consultancies, stock ownership, equity interest, patent/licensing arrangements, etc.) that might pose a conflict of interest in connection with the submitted manuscript.

Manuscript received: 01-13-2023
Revised manuscript received: 03-28-2023
Accepted for publication: 04-14-2023

Free full manuscript:
www.painphysicianjournal.com

Background: Patients with persistent somatoform pain disorder (PSPD) are not uncommon. Still, the disease diagnosis relies primarily on structured interviews, with no objective indicators yet available to aid in the diagnosis. This has led to low diagnostic rates and overconsumption of health care resources for the disorder. Although there is a large body of research to improve the diagnosis of the condition, there are currently no objective indicators available for diagnosis.

Objectives: The aim of this study is to investigate the clinical value of infrared thermography (IRT) for diagnosing PSPD.

Study Design: This is a retrospective study.

Setting: A single academic hospital, outpatient setting.

Methods: The clinical data of patients diagnosed with PSPD in the Pain Department of the First Affiliated Hospital of the Army Medical University from September 2020 to September 2022 were analyzed. The differences in IR thermograms between PSPD patients and healthy controls were analyzed, as well as the relationship between the Hamilton Depression Rating Scale, Hamilton Anxiety Scale, Pittsburgh Sleep Quality Index (PSQI) score, Patient Health Questionnaire-15, and Symptom Check List-90 and the differences in IR thermograms of PSPD patients.

Results: The mean squared error, structural similarity measure, different hash, contrast, entropy, inverse variance, and correlation values of the IR thermogram helped to determine PSPD with statistically significant differences ($P < 0.05$). Inverse variance values were weakly negatively correlated with PSQI scores of PSPD patients (r -0.4721, $P < 0.05$).

Limitations: This study was limited by its sample size and retrospective observational design.

Conclusions: IRT analysis is a useful objective method in diagnosis of PSPD, which also provides a new line of thought for studying the pathogenesis of PSPD.

Key words: Persistent somatoform pain disorder, PSPD, thermal imaging, infrared thermography, IRT, image texture characteristics, psychometric variables, image analysis

Pain Physician 2023: 26:E529-E537

Persistent somatoform pain disorder (PSPD) is a psychiatric disorder with a predominance of constant, severe pain that cannot be rationally explained by physiological processes or somatic disorders (1). The disease has a prolonged course, usually lasting more than 6 months, and impairs social functioning (2). Approximately 5% to 7% of the general population have somatic symptom disorders (SSDs) (3). In the fifth edition of the Diagnostic and Statistical Manual of Mental Disorders (DSM-5 [3]), the 3 types of somatization disorders, undifferentiated somatoform disorders, hypochondriasis, and pain disorders, were reclassified as SSDs and illness anxiety disorders. Actually, most clinical application specialists in pain

departments are likely to diagnose the SSD patients with pain disorders sustained for > 6 months as PSPD, for most cite pain as the chief complaint. In the absence of restrictions, PSPD patients exhibit doctor shopping behavior, leading to overuse and overconsumption of health care resources (4). The oversiting of patients with PSPD stems from amplifying their bodily sensations of pain, making them more willing to believe that the disease is physiologically related and hesitated to interview with a psychologist. Also, differences in the patient's culture and level of education can influence the patient's judgment on the questions in some psychological questionnaires (5). Therefore, it is crucial to make a precise diagnosis and give an explanation to the patient using a rational clinical consultation model. A review of previous studies (6,7) found that psychological assessment scales (e.g., Patient Health Questionnaire-15 [PHQ-15], SSD-B Criteria Scale [SSD-12], etc.) are commonly used as an adjunctive diagnostic modality. At the same time, new studies (8,9) have also explored indicators of PSPD objectivity (e.g., magnetic resonance imaging). The former is more influenced by subjectivity. While the latter is controlled by various factors, such as cost, invasiveness, etc., and the research is immature. As such, an inexpensive, objective diagnostic criterion to help diagnose this disease remains worth exploring.

Infrared thermography (IRT) is widely used in pain departments to determine tissue damage in patients. As the body's largest organ, the skin plays an essential role in this process. IRT imaging provides information by mapping the skin's temperature (i.e., IR thermograms). The thermal patterns obtained reflect the underlying physiology of peripheral blood flow regulated by the autonomic nervous system (10). Thus, temperature recordings can quantify changes in sympathetic tension (i.e., surface heat distribution) that are often secondary to injury or other disease processes (11). Ordinary people exhibit a high degree of thermal symmetry between the bilateral sides (2-side temperature difference 0.5 ± 0.3°C) (12), with asymmetric thermal patterns suggestive of disease processes (13). Suzuki et al (14) found that the IRT of brain temperature changes can be used to assess cortical activity and disease states. Symons et al (15) found in a study of Rett syndrome that IRT may be used to assess changes in sympathetic regulation. Previous studies (16,17) have found a link between pain and autonomic dysfunction, which can cause skin temperature changes. We found in the clinical setting that the IR thermograms of PSPD patients showed unsymmetrical, diffused, punctate, or patchy distributed areas of high temperature. There is no direct pathophysiological mechanism now that can explain the phenomenon. This study aimed to determine the value of using IRT to identify the differences between normal human and PSPD patients, which maybe provide an objective method for helping to diagnose PSPD and provide a new line of thought for studying the pathogenesis of PSPD.

Methods

This cross-sectional study was conducted at the Pain Department of the First Affiliated Hospital of the Army Medical University from September 2020 to September 2022. Inclusion criteria of PSPD objectives as: 1) with pain as the main complaint and lasting for > 6 months; 2) age 18-65 years; 3) laboratory tests and imageological examination excluded related organ disease; and 4) other somatic symptoms meeting DSM-5 diagnostic criteria. Exclusion criteria of PSPD objectives as: 1) depression and/or anxiety associated with chronic somatosensory pain or severe organic disease; 2) with skin diseases or scar in the trunk of body; and 3) other disease that maybe affect skin temperature. Thirty-seven PSPD patients conform to criteria, 20 women and 17 men, aged 18-65 years, who attended the pain unit of the hospital during this period were analyzed for sociodemographic data and standardized questionnaires for psychometric variables (i.e., Hamilton Depression Rating Scale [HAMD]; Hamilton Anxiety Scale [HAMA]; Pittsburgh Sleep Quality Index [PSQI]; PHQ-15; and Symptom Check List-90 [SCL-90]). Twenty-seven healthy individuals, 11 women and 16 men, aged 18-65 years, who had their IR thermograms taken at the pain department for regular physical examination were selected as the control group. The study was approved by the Local Ethics Committee (KY2022169) of the First Affiliated Hospital of the Army Medical University and was conducted according to the Declaration of Helsinki.

Standardized Questionnaire for Psychometric Variables

The HAMD scale, HAMA scale, PSQI sleep scale, PHQ-15, and SCL-90 were all used to assess the severity of somatic symptoms. In this sample, Cronbach's α for HAMA, HAMD, PSQI, PHQ-15, and SCL-90 was 0.941, 0.866, 0.699, 0.780, and 0.950, respectively.

IR Thermogram

Patients were tested using a medical IR camera (MTI-Economy-2013-A type Jiangbei District, Chongq-

ing) in the clinical setting. The temperature of the working environment for map collection is controlled at (24 ± 2)°C, the humidity at 40% to 60%, the room air is in a relatively static state, and there is no light or direct sunlight. The acquisition band is set to 8-12 μm, the frame pixels are 640 bits x 512 bits, the imaging speed is 9 frames/s, and the temperature resolution is 0.01°C. Patients are prohibited to consume alcohol, coffee, tea, and other stimulating beverages from 1 day before the examination, avoid eating too cold or too hot food and being in an intensely cold or hot environment (e.g., direct blowing in the car/air conditioner) for the first one hour, avoid smoking and drinking for the first 30 minutes, and rest for 15-20 minutes after entering the examination room, and dry naturally if sweat is present before examination. The patient faced the IR camera, 2 m away from the lens, in an upright position facing the lens, and acquired one image each of frontal upper body, back upper body, front lower body, and back lower body, with the frontal upper body image selected (as shown in Fig. 1a) (18). Figure 1b,c shows 2 IR thermograms of the upper frontal bodies of a normal patient (left) and a PSPD patient (right). It was observed clinically that the IR thermograms of the chest and abdomen of PSPD patients showed asymmetrical diffuse dotted sheet-like high-temperature areas. According to this feature, the chest and abdomen were selected as the detection area, with the line connecting the midpoint of the clavicles bilaterally above the anterior trunk, the navel level bilaterally below, and a rectangular area bordered by the narrowest part of the waist bilaterally on both sides. Convert and remap the temperature maps in different colors linearly to 256-level grayscale images. Based on this feature, mean squared error (MSE) values, structural similarity measure (SSIM) values, and different hash (dHash) values of the bilateral IR thermograms of the chest and abdomen of patients and normal patients were calculated separately to compare the differences between the 2 sides, as well as the image texture features (i.e., energy [ASM], entropy [ENT], contrast [CON], correlation [COR], and inverse variance [H]) calculated based on the grayscale covariance matrix to compare the temperature distribution characteristics (19,20).

1) MSE calculates the squared sum of the difference between the 2 sides of the body by one symmetry point. The value of MSE is 0, which means that the temperature values on both sides are identical, and the value of MSE increases as the temperature difference increases (21).

   MSE=1/mn ∑_(i=0)^(m-1)▒∑_(j=0)^(n-1)▒〖[I(i,j)-K(i,j)]〗^2

   The m and n distributions represent the width and height of the image, and I and K represent the pixel values of the 2 images, respectively.
2) SSIM is used to calculate the brightness, contrast, and structural difference of the IR heat map; if the temperature values of both sides are the same, it reflects that the images are precisely the same and the SSIM is 1. The closer the SSIM is to 1, the smaller the temperature difference between the 2 sides (21,22).

   SSIM(x,y)=((2μ_x μ_y+C1)(2σ_xy+C2))/((μ_x^2+μ_y^2+C1)(σ_x^2+σ_y^2+C2))

   Where μx denotes the mean value in the x-direction in the image, σx denotes the variance in the x-direction. In contrast, μy and σy represent the mean and variance in the y-direction in the picture, respectively. C1 and C2 distributions denote the mean pixel intensity of the 2 images, and σxy represents the covariance values in the x- and y-directions (22).
3) dHash algorithm is an algorithm to calculate the image similarity; when the more similar the IR heat map on both sides is, the closer the dHash value is to 100%. Where the Hamming distance in this algorithm is the number of steps needed to turn a set of binary data into another collection of data, this value can measure the difference between 2 pictures; the smaller the Hamming distance, the higher the similarity. dHash's Hamming distance calculation steps are: first compress the picture into a small 9*8 image, then convert it into a grayscale image; dHash algorithm works between adjacent pixels, each row of 9 pixels produces 8 different differences, a total of 8 rows, then 64 difference values are generated, or 32-bit 01 string; get the fingerprint: if the left pixel is brighter than the right, it is recorded as 1; otherwise it is 0; then calculate the Hamming distance by the dHash value (25).
4) ASM in the image texture feature responds to the uniformity of temperature distribution; the more concentrated the temperature, the greater the energy.

   Asm=∑_i▒∑_j▒〖[P〖(i,j)〗]^2 〗
5) Con responds to the degree of difference between the regional temperature and the surrounding area. The greater the difference, the greater the contrast.

   Con=∑_i▒∑_j▒〖(i-j)^2 P(i-j)〗

6) Ent responds to the dispersion of different temperatures; the more significant the dispersion, the greater the entropy value.
   Ent=-∑_i▒∑_j▒〖P(i,j)logP(i,j)〗
7) H responds to the trend of regional temperature change, and the slower the change, the larger the value.
   H=∑_(i=0)^(N=1)▒∑_(j=0)^(N=1)▒(P(i,j|d,θ))/(1+〖(i-j)〗^2)
8) COR responds to the consistency of temperature distribution. The image temperature is uniform and equal; the more significant the correlation value, the larger the correlation value.
   Cor=([∑_i▒∑_j▒〖(ij)P(i,j)-μ_x μ_y 〗])/(σ_x σ_y)
   In the above equations, 4-8, i and j both denote the gray level of 2 pixels, d represents the step size, θ denotes the position relationship of the pixel pair, σx denotes the variance in the x-direction, and σy means the variance in the y-direction; μx, μy indicate the mean values of x- and y-directions in the image (21,26).

Statistical Method

IBM SPSS 26.0 software (IBM Corporation, Armonk, NY) was used to analyze the collected data statistically. Measures were expressed as mean ± standard deviation (SD) (X ± ð) with a t test; data were first tested for normality distribution; then correlation analysis was performed using binary logistic regression and Pearson or Spearman correlation according to the type of distribution. The Pearson correlation coefficient r can be classified as uncorrelated ($0 \le |r| < 0.3$), weakly correlated ($0.3 \le |r| < 0.5$), moderately correlated ($0.5 \le |r| < 0.8$), and strongly correlated ($0.8 \le |r| < 1$) based on the values. Receiver operating characteristic (ROC) curves were used to determine the best split point based on cutoff values. MedCalc 20.0 (MedCalc Software bvba, Ostend, Belgium) was applied to test for significant differences between the curves' regions. $P < 0.05$ was considered a statistically significant difference.

Results

PSPD and Healthy Controls (HC) in general

There were no significant differences between PSPD and HC in terms of age, gender, married, or education for the comparison. The mean age of the patients was 41.8 years (SD = 12.0). Approximately half were women. The majority indicated that they had > 9 years of schooling. Table 1 demonstrates the demographic characteristics of the sample. There were no significant differences in any of the demographic factors (Table 1).

The Eigenvalue Situation of the IR Thermogram

MSE, SSIM, dHash, Con, Ent, H, and COR values were significantly correlated with PSPD. B > 1, odds ratio > 1 for MSE, Con, and Ent, suggests that the greater the value of these 3, the greater the likelihood of PSPD. The smaller the remaining indicators, the higher the likelihood of PSPD (Table 2).

Diagnostic Accuracy

Table 3 shows the predictive values and efficiency rates for sensitivity and specificity. The best cutpoint was established by calculating the total score of MSE, SSIM, dHash, Con, Ent, H, and COR values.

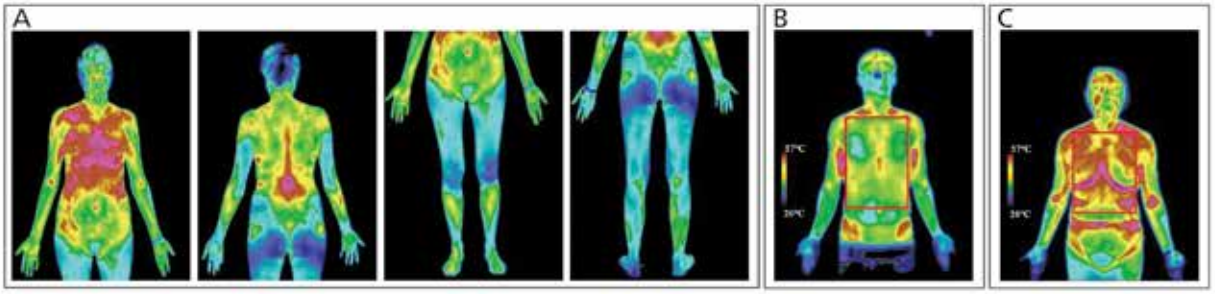

Fig. 1. *A. Infrared thermograms of the frontal upper body, back upper body, front lower body, and back lower body of the human being; B. Infrared thermogram of the human body for ordinary people, and C. for PSPD (persistent somatoform pain disorder) patients. The temperature distribution of infrared thermograms in ordinary people is almost symmetrical, while the graphs of PSPD patients show the irregular distribution of high-temperature regions on the chest and abdomen.*

For MSE values, the efficiency was 94.3% at the cutpoint of 1,328. The sensitivity is 88.5%, the specificity is 94.6%. For SSIM values, 93% efficiency was highest at cutpoints > 0.52. Sensitivity is 92.3%, specificity is 86.5%. For dHash values, 68% efficiency was highest at cutpoints > 0.55. The sensitivity was 53.9%, and the specificity was 75.7%. For Con values, the efficiency was 68% at the cutpoint of 0.4005. The sensitivity is 76.9%, the specificity is 54%. For Ent values, 74% efficiency was highest at cutpoints < 3.186. Sensitivity is 96.15%, specificity is 51.35%. For H values, 68% efficiency was highest at cutpoints > 0.8025. The sensitivity was 88.46%, and the specificity was 46%. For COR values, 83% efficiency was highest at cutpoints >

Table 1. *Baseline data of the study sample (n=64).*

Variable	Total (n=64) (X±σ)/n (%)	Ordinary People (n=27) (X±σ)/n (%)	PSPD (n=37) (X±σ)/n (%)	T	*P* value
Age	41.8 ± 12.0	43.0 ± 15.6	40.7 ± 12.2	0.696	> 0.05
Women	31 (48%)	11 (41%)	20 (54%)	1.871	> 0.05
Education				0.225	> 0.05
< 9 years	35 (54%)	14 (52%)	20 (54%)		
> 9 years	30 (46%)	13 (48%)	17 (46%)		

Abbreviation: PSPD, persistent somatoform pain disorder.

Table 2. *Correlation with PSPD.*

	B	Standard Error	Significance	OR	95% CI for Exponent (B)	
					Lower	Upper
MSE	0.005	0.001	0.000	1.005	1.003	1.008
Constant	-7.103	1.834	0.000	0.001		
SSIM	-22.599	5.633	0.000	0.000	0.000	0.000
Constant	12.075	3.018	0.000	175352.468		
dHash	-6.299	2.697	0.020	0.002	0.000	0.363
Constant	3.681	1.461	0.012	39.679		
Con	6.243	2.645	0.018	514.455	2.881	91875.206
Constant	-2.141	1.059	0.043	0.117		
Ent	3.481	1.403	0.013	32.498	2.080	507.787
Constant	-10.302	4.299	0.017	0.000		
H	-20.432	8.878	0.021	0.000	0.000	0.048
Constant	17.187	7.338	0.019	29134355.689		
COR	-0.088	0.023	0.000	0.916	0.876	0.958
Constant	10.472	2.654	0.000	35328.849		

Abbreviations: PSPD, persistent somatoform pain disorder; OR, odds ratio; CI, confidence interval; MSE, mean squared error; SSIM, structural similarity measure; dHash, different hash; Con, contrast; Ent, entropy; H, inverse variance; COR, correlation.

Table 3. *Cutoff values, sensitivity, specificity, efficiency and Youden index (max) of several meaningful indicators.*

	Cutoff Value	Sensitivity (%)	Specificity (%)	Efficiency (%)	Youden Index (max)
MSE	1,328	88.5%	94.6%	94.3%	0.8305
SSIM	0.52	92.3%	86.5%	93%	0.788
dHash	0.55	53.9%	75.7%	68%	0.2953
Con	0.4005	76.9%	54.0%	68%	0.3097
Ent	3.186	96.15%	51.35%	74%	0.475
H	0.8025	88.46%	46%	68%	0.3441
COR	127.5	53.85%	100%	83%	0.5385

Abbreviations: MSE, mean squared error; SSIM, structural similarity measure; dHash, different hash; Con, contrast; Ent, entropy; H, inverse variance; COR, correlation.

127.5. The sensitivity was 53.85%, and the specificity was 100%.

ROC Analysis

As shown in Fig. 2 and Table 4, MSE values (area under the curve [AUC] = 0.943; $P < 0.05$; 95% confidence interval [CI] = 0.886-0.999), SSIM values (AUC = 0.931; $P < 0.001$; 95% CI = 0.870-0.992), and COR values (AUC = 0.831; $P < 0.05$; 95% CI = 0.729-0.932) showed good individual diagnostic accuracy. dHash values (AUC = 0.676; $P < 0.05$; 95% CI = 0.5407-0.812), Con values (AUC = 0.678; $P < 0.005$; 95% CI = 0.547-0.809), Ent values (AUC = 0.735; $P < 0.05$; 95% CI = 0.612-0.858), and H values (AUC = 0.678; $P < 0.05$; 95% CI = 0.548-0.809) showed moderate individual diagnostic accuracy. The results of the 2-way comparison of AUC by MedCalc are shown in Table 5. The diagnostic accuracy of MSE and SSIM indexes was more excellent than other indexes (except between SSIM and COR), but there was no significant difference between them; the diagnostic accuracy of COR was greater than that of Con and H, and there was no significant difference between all the remaining indexes.

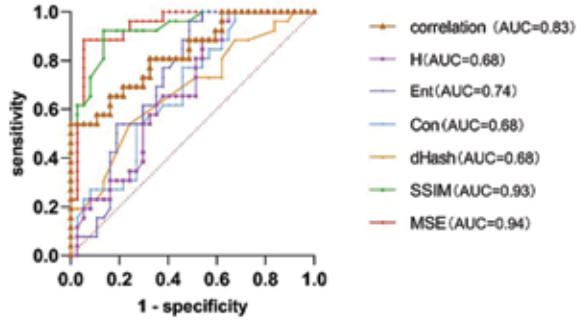

Fig. 2. *Receiver operating characteristic curves of MSE, SSIM, dHash, Con, Ent, H, correlation s in detecting the diagnosis of PSPD.*
MSE: Mean Squared Error; SSIM: Structural Similarity Measure; dHash: Different Hash; Con: constrast; Ent, entropy; H, inverse variance; COR, corelation.

The Relationship Between MSE, SSIM, dHash, Con, Ent, H, and COR Values of IR Thermograms and HAMD, HAMA, PSQI, PHQ-15, and SCL-90 Scores

The appeal indexes were tested for normal distribution, in which SSIM, dHash value, H, HAMA, HAMD, and PSQI conformed to the normal distribution, and the rest did to skewed distribution. Correlation analysis was performed, and it found that only H was correlated with PSQI. In Fig. 3, H was negatively correlated with PSQI, suggesting that the greater the patient's PSQI score, the smaller the H value, indicating a greater regional temperature change, with an R-value of -0.4721, the 2 were weakly correlated.

Discussion

The prevalence of PSPD is gradually increasing, while the pathogenesis remains unclear, and also the low diagnostic rate contributes to the ineffective treatment of the condition. This study firstly evaluated the diagnostic value of IR thermographic characteristic values for PSPD in pain departments. The results showed that all these indicators, i.e., MSE, SSIM, dHash, Con, Ent, H, and COR values, were helpful screening feature values. It is further demonstrated that it is meaningful to use these indicators of IRT to improve the diagnostic rate of PSPD.

In this study, our team calculated these indicators based on the symmetry of the human body surface

Table 4. *AUC area of MSE, SSIM, and meaningful image texture feature values.*

	AUC	Standard Error[a]	Asymptotic Significance[a]	Asymptotic 95% CI	
				Lower Bound	Upper Bound
MSE	0.943	0.029	0.000	0.886	0.999
SSIM	0.931	0.031	0.000	0.870	0.992
dHash	0.676	0.069	0.018	0.5407	0.812
Con	0.678	0.067	0.017	0.547	0.809
Ent	0.735	0.063	0.002	0.612	0.858
H	0.678	0.067	0.016	0.548	0.809
COR	0.831	0.052	0.000	0.729	0.932

Abbreviations: CI, confidence interval; MSE, mean squared error; SSIM, structural similarity measure; dHash, different Hash; Con, contrast; Ent, entropy; H, inverse variance; COR, correlation; AUC, area under the curve.
aUnder the nonparametric assumption

Table 5. *Two-way comparison of AUC results for each index.*

	SSIM	dHash	Ent	Con	H	COR
MSE	$P > 0.05$*	$P < 0.05$	$P < 0.05$	$P < 0.05$	$P < 0.05$	$P < 0.05$
SSIM		$P < 0.05$	$P < 0.05$	$P < 0.05$	$P < 0.05$	$P > 0.05$*
dHash			$P > 0.05$*	$P > 0.05$*	$P > 0.05$*	$P > 0.05$*
Ent				$P > 0.05$*	$P > 0.05$*	$P > 0.05$*
Con					$P > 0.05$*	$P < 0.05$
H						$P < 0.05$

*$P > 0.05$, differences between AUCs were not statistically significant.
Abbreviations: SSIM, structural similarity measure; dHash, different hash; Ent, entropy; Con, contrast; H, inverse variance; COR, correlation; MSE, mean squared error; AUC, area under the curve.

temperature distribution. The results suggest that the larger the indexes, i.e., MSE, Con, and Ent, the more likely they will be screened as PSPD, and the opposite for the other remaining indicators. This result is consistent with previous studies (12,27), which concluded that PSPD patients have a disturbed and asymmetric body surface temperature distribution. However, this study did not show a correlation between the severity of the disease and temperature disturbance, which warrants further investigation. At the same time, we correlated several scales that can reflect somatic symptoms and emotions with the indicators. We found that only H was negatively and weakly associated with PSQI, demonstrating that the smaller the H value, the higher the PSQI score and the higher the likelihood of PSPD. This result suggests that PSPD patients have poorer sleep quality, a finding consistent with previous studies (28,29) that PSPD patients often have sleep disturbances. In addition, Löwe et al (30) indicated that most patients with PSPD tend to have depression and/or anxiety. This study did not yield an association between diagnostic indicators and these 2 scales, suggesting that depression or anxiety is not exclusively present in PSPD patients, in line with Löwe et al (30). These indicators also did not correlate with the scales reflecting somatic symptoms. Because they can only determine whether the disease is present, but cannot evaluate the severity of the disease and the patient's discomfort, judging the severity based on the magnitude of the indicators would be a significant research direction.

Unlike previous studies, this is the first study to analyze PSPD from an IR thermogram rather than a subjective scale and clinical interviews. This study can yield objective indicators for diagnosing PSPD. In the past, clinical interviews were used to diagnose these patients, but the results were not promising, so new ways of interpreting the disease are still being explored. Abasia et al (7) used the SSD-12 as a screening

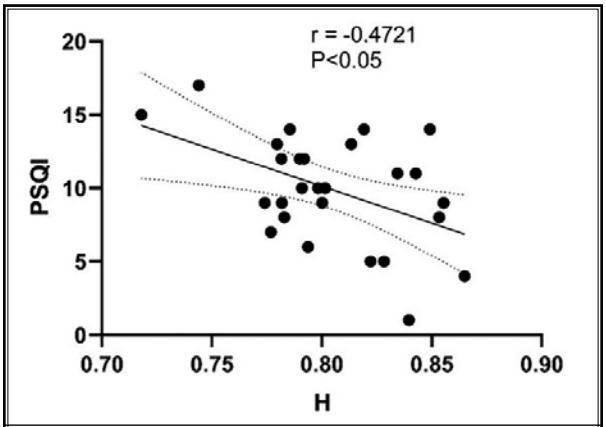

Fig. 3. *Correlation of Pittsburgh Sleep Quality Index (PSQI) with inverse variance (H). With an R-value of -0.4721, the two were negatively and weakly correlated.*

tool for SSDs with a critical value > 14 as optimal, a sensitivity of 70.83%, and a specificity of 70.07%. Toussaint et al (29) yielded an AUC of 0.70; 95% CI = 0.65-0.76 for PHQ-15; 0.71; 95% CI = 0.66-0.77 for Somatic Symptom Scale-8; and 0.74; 95% CI = 0.69-0.80 for SSD-12. The combination of the above questionnaires improves the diagnostic accuracy for diagnosing PSPD. The above studies all started from the scale and were closely linked to the patient's subjective quizzes, which are informative for physicians' clinical diagnosis, but still lead to misdiagnoses. Also, because patients with the disease are often seen in various departments believing it is physiologically related, physicians cannot convince patients that they do not have organic changes by relying on interviews and scale assessments. The present study does not base its results on patients' subjective thoughts. It analyzes directly from the actual taken IR thermograms, which are more objective than the scales and, at the same time, can easier convince the patients. There are also neuroimaging studies (31) available for

this disease. Still, the tests are expensive and physically damaging for the patient; whereas, IRT has the advantage of being less expensive and noninvasive.

Patients with SSDs are often associated with autonomic dysfunction (32). The sympathetic nerves control the sweat glands and the blood vessels under the skin. Sympathetic nerves control the constriction and relaxation of skin blood vessels, thereby controlling blood flow to the skin. The blood flowing through the skin can bring the heat inside the body, dissipating through the skin's surface. When sympathetic nerves are excited, sweat glands secrete sweat, and skin blood vessels constrict (33). Huijie et al (32) revealed that a sympathetic skin response (SSR) in patients with SSDs differs from normal individuals, and an SSR is closely related to prosweating (32). The temperature of the human skin surface results from a combination of heat production and heat dissipation, and sweat enables the body to evaporate and dissipate heat. Changes in blood flow caused by the relaxation and contraction of blood vessels under the skin can also affect the heat dissipation of the skin. Therefore, it is speculated that the autonomic nervous function disorder of patients with SSD leads to the difference in the temperature distribution on the skin surface of the patients with that of ordinary people. This hypothesis could explain the asymmetry of temperature distribution on IR thermograms in patients with PSPD. In addition, other patients with chronic pain also show asymmetrical IR thermographic temperatures, as well as causing sympathetic disturbances, but with a different degree and presentation than that of patients with PSPD. Therefore, it is impossible to explain the mechanism of their temperature variation characteristics by solely autonomic dysfunction. Limitations of the trial were the limited number of IR thermograms that were obtained and the limited features of them that were analyzed. Actually, there are still other more valuable features in the PSPD patients' IR thermograms that can be explored in the future. In the trial design, all patients enrolled were diagnosed definitively by modified DSM-5 criteria firstly and excluded if they had other comorbidities. Because of this design approach, it is uncertain whether patients with PSPD containing coexisting disease can be screened out when using IRT alone. This study only provides a new idea for the diagnosis of PSPD, and further research is needed to investigate the pathophysiological mechanisms of the disorder. At a later stage, an artificial intelligence pattern recognition software for PSPD can be designed for clinical screening of PSPD using convolutional neural networks when the sample size is larger, based on several eigenvalues derived from this study as a basis (34,35). Clinicians will use it for clinical screening of PSPD and evaluating the effect of treatment. The pattern recognition software will assist clinicians in improving the identification rate of PSPD, avoiding repeated patient visits and wasting of medical resources.

Conclusions

IRT, as a noninvasive test, is simple to perform and can better screen patients with PSPD. Based on our analysis, when MSE > 1,328, Con > 0.4005, and Ent > 3.186, the IR thermogram suggested that the examined patients tended to be PSPD patients, while when SSIM < 0.52, dHash < 0.55, H < 0.8025, and COR < 127.5, the results favored the diagnosis of PSPD. Therefore, we believe that clinicians can significantly improve the diagnostic rate by using the objectivity derived from this study to aid in diagnosing this disorder.

Acknowledgments

We thank all the patients and investigators involved in this study. We thank Professor Yujie Lei (Army Medical University, China) for the help on statistical analyzing and Dr. Junlong Li (Johannes Gutenberg-Universität Mainz, Germany) on the amendment of manuscript writing.

References

1. Luo YL, Heeramun-Aubeeluck A, Huang X, et al. Factors influencing quality of life in Chinese patients with persistent somatoform pain disorder. *Psychol Health Med* 2014; 19:744.
2. Cooper JE (ed), World Health Organization Geneva. *Pocket guide to ICD-10 classification of mental and behavioural disorders: With glossary and diagnostic criteria for research: ICD-10/DCR-10.* APA Publishing, Washington, DC 1994.
3. Organization AP. *Diagnostic and statistical manual of mental disorders.* Fifth edition. APA Publishing, Washington, DC 2013.
4. Peng TA, Ma YA, Jh B, et al. Clinical and psychobehavioral features of outpatients with somatic symptom disorder in otorhinolaryngology clinics. *J Psychosom Res* 2021; 148:110550.
5. Naskar C, Grover S, Sharma A, Padhy SK. A comparison of patients with somatic symptom disorder attending psychiatric services and those unwilling to attend psychiatric services. *Asian J Psychiatr* 2020; 53:102163.
6. Kocalevent RD, Hinz A, Brähler E. Standardization of a screening

instrument (PHQ-15) for somatization syndromes in the general population. *BMC Psychiatry* 2013; 13:91.

7. Abasia I, Ghapanchia A, Toussaintb A, et al. Psychometric properties of the Persian version of the somatic symptom disorder–B Criteria Scale (SSD-12) in community and clinical samples. *Gen Hosp Psychiatry* 2022; 78:1-8.
8. Huang T, Zhao Z, Yan C, et al. Altered spontaneous activity in patients with persistent somatoform pain disorder revealed by regional homogeneity. *PLoS One* 2016; 11:e0151360.
9. Sun X, Pan X, Ni K, et al. Aberrant thalamic-centered functional connectivity in patients with persistent somatoform pain disorder. *Neuropsychiatr Dis Treat* 2020; 16:273-281.
10. Nola IA, Kolanc D (eds). *Thermography in biomedicine.* In: ELMAR-International Symposium Electronics in Marine, Zadar, Croatia, 2015, pp. 17-20.
11. Fernández-Cuevas I, Marins JCB, Lastras JA, et al. Classification of factors influencing the use of infrared thermography in humans: A review. *Infrared Physics Tech* 2015; 71:28-55.
12. Vardasca R, Ring F, Plassmann P, Jones C. Termal symmetry of the upper and lower extremities in healthy subjects. *Thermology International* 2012; 22:53-60.
13. Alfieri FM, Massaro AR, Filippo TR, Portes LA, Battistella LR. Evaluation of body temperature in individuals with stroke. *NeuroRehabilitation* 2017; 40:119-128.
14. Suzuki T, Oishi N, Fukuyama H. Simultaneous infrared thermal imaging and laser speckle imaging of brain temperature and cerebral blood flow in rats. *J Biomed Optics* 2019; 24:1-11.
15. Symons FJ, Byiers B, Hoch J, et al. Infrared thermal analysis and individual differences in skin temperature asymmetry in Rett Syndrome. *Pediatr Neurol* 2015; 53:169-172.
16. Brelsford KL, Uematsu S. Thermographic presentation of cutaneous sensory and vasomotor activity in the injured peripheral nerve. *J Neurosurg* 1985; 62:711-715.
17. Gandhavadi B, Rosen JS, Addison RG. Autonomic pain. *Postgrad Med* 1982; 71:85-90.
18. Moreira DG, Costello JT, Brito CJ, et al. Thermographic imaging in sports and exercise medicine: A Delphi study and consensus statement on the measurement of human skin temperature. *J Thermal Biol* 2017; 69:155-162.
19. Naganawa S, Enooku K, Tateishi R, et al. Imaging prediction of nonalcoholic steatohepatitis using computed tomography texture analysis. *Euro Radiol* 2018; 28:3050-3058.
20. Chunmei X, Mei H, Yan Z, Haiying W. Diagnostic method of liver cirrhosis based on MR image texture feature extraction and classification algorithm. *J Med Syst* 2019; 44:11.
21. Yan X, Gilani SZ, Qin H, Mian A. Structural similarity loss for learning to fuse multi-focus images. *Sensors* 2020; 20:6647.
22. Umbaugh SE. *Digital image processing and analysis: Applications with MATLAB and CVIPtools*, Third Edition. CRC Press, Boca Raton, FL 2018.
23. Hasan M, El-Sakka MR. Improved BM3D image denoising using SSIM-optimized Wiener filter. *EURASIP J Image Video Process* 2018; 2018:25.
24. Peng J, Shi C, Laugeman E, et al. Implementation of the structural SIMilarity (SSIM) index as a quantitative evaluation tool for dose distribution error detection. *Med Phys* 2020; 47:1907-1919.
25. Chang YN, Chang HH, Liu F, Lee DH, Lagoa R, Kumar S. Automatic brain MR image denoising based on texture feature-based artificial neural networks. *Biomed Mater Eng* 2015; 26(suppl 1):S1275.
26. Qiu H, Wang D, Miao H. Analysis of the effect of robots in the treatment of pancreatic cancer based on smart medicine. *J Healthc Eng* 2021; 2021:9734882.
27. Power JD, Perruccio AV, Badley EM. Pain as a mediator of sleep problems in arthritis and other chronic conditions. *Arthritis Rheum* 2010; 53:911-919.
28. Niu HH, Lui PW, Hu JS, et al. Thermal symmetry of skin temperature: Normative data of normal subjects in Taiwan. *Zhonghua Yi Xue Za Zhi (Taipei)* 2001; 64:459-468.
29. Löwe B, Spitzer RL, Williams JBW, Mussell M, Schellberg D, Kroenke K. Depression, anxiety and somatization in primary care: Syndrome overlap and functional impairment. *Gen Hosp Psychiatry* 2008; 30:191-199.
30. Dong L, Liang HB, Du J, et al. Microstructural differences of the cerebellum-thalamus-basal ganglia-limbic cortex in patients with somatic symptom disorders: A diffusion kurtosis imaging study. *Cerebellum* 2022.
31. Aigner M, Graf A, Freidl M, et al. Sleep disturbances in somatoform pain disorder. *Psychopathology* 2003; 36:324-328.
32. Huijie B, Hailong W, Yanfang Z. Analysis of sympathetic skin response in patients with somatization disorder. *Chinese Community Physician* 2021; 37:11-12.
33. Srinivasu PN, Sivasai JG, Ijaz MF, Bhoi AK, Kim W, Kang JJ. Classification of skin disease using deep learning neural networks with MobileNet V2 and LSTM. *Sensors* 2021; 21:2852.
34. Ohmi M. Application to skin physiology using optical coherence tomography. *Laser Therapy* 2016; 25:251-258.
35. Shin HC, Roth HR, Gao M, et al. Deep convolutional neural networks for computer-aided detection: CNN architectures, dataset characteristics and transfer learning. *IEEE Trans Med Imaging* 2016; 35:1285-1298.